

REFORM: Removing False Correlation in Multi-level Interaction for CTR Prediction

Songli Wu^{1*} Liang Du^{2*} Jia-Qi Yang^{1*} Yuai Wang³ De-Chuan Zhan^{1†}
Shuang Zhao² Zi-Xun Sun²

¹ State Key Laboratory for Novel Software Technology, Nanjing University, China

² Interactive Entertainment Group, Tencent Inc., China

³ Fudan University, China

Abstract

Click-through rate (CTR) prediction is a critical task in on-line advertising and recommendation systems, as accurate predictions are essential for user targeting and personalized recommendations. Most recent cutting-edge methods primarily focus on investigating complex implicit and explicit feature interactions. However, these methods neglect the issue of false correlations caused by confounding factors or selection bias. This problem is further magnified by the complexity and redundancy of these interactions. We propose a CTR prediction framework that **RE**moves **F**alse **c**ORrelation in **M**ulti-level feature interaction, termed **REFORM**. The proposed REFORM framework exploits a wide range of multi-level high-order feature representations via a two-stream stacked recurrent structure while eliminating false correlations. The framework has two key components: I. The multi-level stacked recurrent (MSR) structure enables the model to efficiently capture diverse nonlinear interactions from feature spaces of different levels, and the richer representations lead to enhanced CTR prediction accuracy. II. The false correlation elimination (FCE) module further leverages Laplacian kernel mapping and sample reweighting methods to eliminate false correlations concealed within the multi-level features, allowing the model to focus on the true causal effects. Extensive experiments based on four challenging CTR datasets and our production dataset demonstrate that the proposed REFORM model achieves state-of-the-art performance. Codes, models and our dataset will be released at <https://github.com/yansuoyuli/REFORM>.

1 Introduction

In recent years, recommendation systems based on user behaviours and feature modelling have significantly enhanced the precision of recommendations in advertising and online retail applications. Click through rate

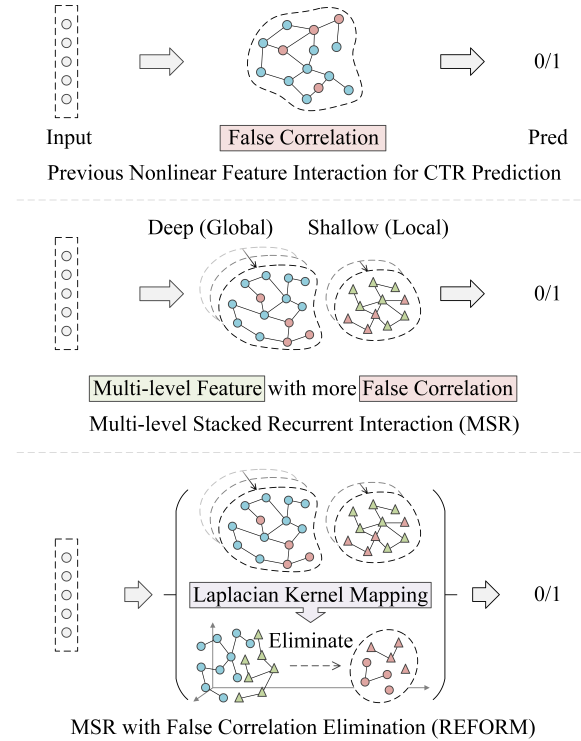


Figure 1: REFORM exploits multi-level features with false correlation elimination to enhance CTR prediction.

(CTR) estimation is a fundamental task in recommendation systems. To more accurately capture user interests, richer features can be extracted, which has emerged as one of the foremost and pivotal topics in the field of recommendation systems. To learn richer feature interactions, various models have been developed. On the one hand, [27, 17, 14, 23] learn low-order feature interactions to achieve low time and space complexity. However, using only first-order and second-order feature interactions may limit performance [9]. On

*indicates equal contribution.

†Corresponding authors: zhandc@nju.edu.cn.

the other hand, xDeepFM [12] and AutoInt [21] aim to capture high-order feature interactions. Methods with two-stream structure design such as DCN [24] automate feature cross-coding with linear and nonlinear feature learning streams. FinalMLP [13] adopts two nonlinear feature learning streams and encodes the features of different streams by setting the multilayer perceptron (MLP) with different parameters, which achieves better performance than models with combinations of linear and nonlinear streams. Although using a two-stream MLP structure with different parameters and stacking depths can construct different nonlinear feature spaces to some extent, our experimental analysis reveals that by utilizing a more sophisticated two-stream structure, there is still significant room for performance improvement, as discussed in Sections 4.3.

Inspired by the above analysis, we introduce a multi-level stacked recurrent (MSR) structure featuring both shallow and deep nonlinear feature learning streams. Previous works such as [5] have proven that the stacked recurrent structure can learn more complex representations by adding depth to the model, and each layer can potentially learn to represent different levels of abstraction. With restoring the previous state, more stacks lead to better integration of global high-level contextual representations (e.g., potential relationships between users and items), and fewer stacks lead to more combinations of features with local details (e.g., user characteristics). Therefore, we construct a two-stream network based on the stacked recurrent structure to exploit the network’s ability to capture both global and local features. A practical method is further introduced to improve the efficiency of the MSR (in Section 3.1).

Furthermore, as illustrated in Figure 1 (Rows 1), previous nonlinear interaction-based methods are hindered by the presence of “False Correlation” in their representations. False correlation refers to a statistical relationship between two or more variables that appears to be causal but is not. This can occur due to confounding factors or selection bias [31]. For example, an advertisement recommendation system may observe a correlation between the purchase of yoga mats and game consoles. However, this perceived correlation could be false, as the co-occurrence of purchases may be attributed to the individual popularity of each item rather than a genuine underlying relationship between the two products. Consequently, effective recommendations require distinguishing between correlation and causality, where correlation signifying associations and causality revealing cause-and-effect relationships. As shown in Figure 1 (Row 2), the incorporation of multi-level feature combinations could potentially increase the number of false correlations, because the false

correlations are also hidden in the combinations of features at different levels. Many recent approaches only consider increasing the diversity of feature interactions, but ignore that the diversity may lead to more false correlations. Consequently, we first take the problem of false correlations in multi-level feature interactions into account. As shown in Figure 1 (Row 3), to address this critical issue, we employ the Laplacian kernel function to project low-dimensional feature interactions into a high-dimensional space. Thus, nonlinear transformations can be achieved in the low-dimensional space through a linear transformation in the high-dimensional space. Then, we use a sample reweighting strategy that learns different weights for each instance during training to eliminate false correlations. The detailed theory will be explained in Section 3.5.

Compared to previous nonlinear interaction-based methods, our method not only effectively constructs multi-level features through an efficient two-stream stacked recurrent structure, but also solves the false correlation issues concealed within hierarchical features, which fundamentally enhances the CTR prediction, rendering it suitable for practical applications. Our contributions are summarized as follows:

- We propose a CTR prediction framework that removes false correlation in multi-level feature interaction (REFORM), which leverages critical causal relationships between items and users in diverse nonlinear feature spaces to enhance the CTR prediction.
- We propose a multi-level stacked recurrent (MSR) structure, which efficiently builds multi-level feature spaces to obtain both global and local representations.
- We introduce a false correlation elimination (FCE) module, which utilizes Laplacian kernel mapping and sample reweighting methods to eliminate false correlations hidden in multi-level feature spaces.
- The results of extensive experiments based on four challenging CTR datasets and our production dataset demonstrate that REFORM achieves state-of-the-art performance.

2 Related works

2.1 Click through rate prediction CTR prediction plays an important role in online advertising, and the use of deep neural networks (DNNs) has notably enhanced predictive performance. Nevertheless, it is worth noting that these models [21, 2, 30, 3, 25, 34, 13], despite their advancements, may inadvertently incorpo-

rate false correlation during training, potentially influencing overall performance [19].

2.2 Recurrent structure Recurrent structures have found widespread application in various research fields, including computer vision (CV) and natural language processing (NLP). For instance, in stereo matching, a recurrent hourglass network was proposed by [5], effectively capturing multi-level information. This enhances the network’s adaptability to complex scenarios by leveraging comprehensive global and local features. In the realm of recommendation systems, DRIN [10] employed a recurrent neural network (RNN) with 1×1 convolution kernels to recurrently model second-order feature interactions between the raw feature and the current feature. However, DRIN utilizes only a single vanilla RNN branch, overlooking the potential benefits of a two-stream structure with varying stacking depths for capturing both global and local feature representations simultaneously. In contrast, our two-stream MSR is equipped with self-attention mechanism, attenuation units, and an acceleration method. This design fundamentally enhances the network’s capacity to efficiently capture multi-level high-order features.

2.3 Casual inference In the field of causal inference, causality refers to the cause-effect relationship between variables, where changes in one variable trigger changes in another. The objective is to identify these relationships. On the other hand, false correlation refers to an observed association that does not necessarily indicate a genuine causal connection, often due to confounding variables or selection bias. [4] utilized feature decorrelation to promote feature independence, thereby reducing textual spurious correlations for natural language understanding. [32] employed sample reweighting for variable decorrelation to identify stable features for image classification. [11] incorporated causal inference into recommendation systems to tackle the issue of selection bias. However, their approach is primarily focused on factorization machine-based (FM) models, and their efficiency is hindered by the optimization method, especially when handling a large number of features. To the best of our knowledge, we are the first to identify and address the issue of false correlation in multi-level higher-order feature interactions in CTR prediction.

3 Method

3.1 Multi-level stacked recurrent interaction (MSR) The proposed MSR contains two streams: the deep stacked recurrent stream (D-SR) and the shallow stacked recurrent stream (S-SR). As shown in Figure 2,

each stream includes multiple stacked recurrent blocks with a self-attention structure and varying attenuation coefficients, which enhances the depth-based pattern and dependency learning. The input feature of both D-SR and S-SR is denoted as x_0 , and the outputs of D-SR and S-SR are denoted as F_d and F_s , respectively. The calculation process is defined as: $F_d = \text{D-SR}(x_0)$, $F_s = \text{S-SR}(x_0)$. We take the i -th block of the D-SR as an example. Given an input x_{i-1} , we first project it into a one-dimensional function w_v : $V_i = x_{i-1} \cdot w_v$ and then map V_i to x_i through the state S_i . We recurrently calculate the output as follows:

$$(3.1) \quad S_i = r_i S_{i-1} + K_i^T V_i,$$

$$(3.2) \quad x_i = \text{SR}_i(x_{i-1}) = Q_i S_i,$$

where SR_i denotes the i -th block, Q_i , K_i , and V_i are projections, r_i is the attenuation coefficient, and $i \in 1, 2, 3, \dots, M$. We further add a swish gate [16] in each stream to increase the non-linearity of the MSR layers.

A practical method to improve the computational efficiency of MSR. In addition, we find that many weights and importance values in softmax are applied to abnormal or null values, which results in unnecessary computational costs. Therefore, we propose to change softmax to learnable matrices, using the stacked recurrent structure with a relative position encoding to reduce time and space costs.

Algorithm 1 The procedure of D-SR

Input: Input data x_0 , Attenuation coefficient r_i , Learnable matrices P_Z , P_U , Blocks number: M

Output: F_d

- 1: $x_1 \leftarrow \text{SR}_1(x_0, r_1)$
 - 2: **for** $i \leftarrow 2$ **to** M **do**
 - 3: $x_i \leftarrow \text{SR}_i(x_{i-1}, r_i)$
 - 4: **end for**
 - 5: $T \leftarrow \text{GroupNorm}([x_1, x_2, \dots, x_M])$
 - 6: $F_d \leftarrow (\text{swish}(x_0 \cdot P_Z) \odot T) \cdot P_U$
 - 7: **return** F_d
-

Formally, we construct the layer as shown in Algorithm 1, where P_Z and P_U are learnable matrices to replace softmax, and “GroupNorm” [20] normalizes the output of each block. In summary, the different depths of D-SR and S-SR lead to significant distinctions in learning feature interactions of any order, which enables the model to grasp global and local dependencies at various abstraction levels.

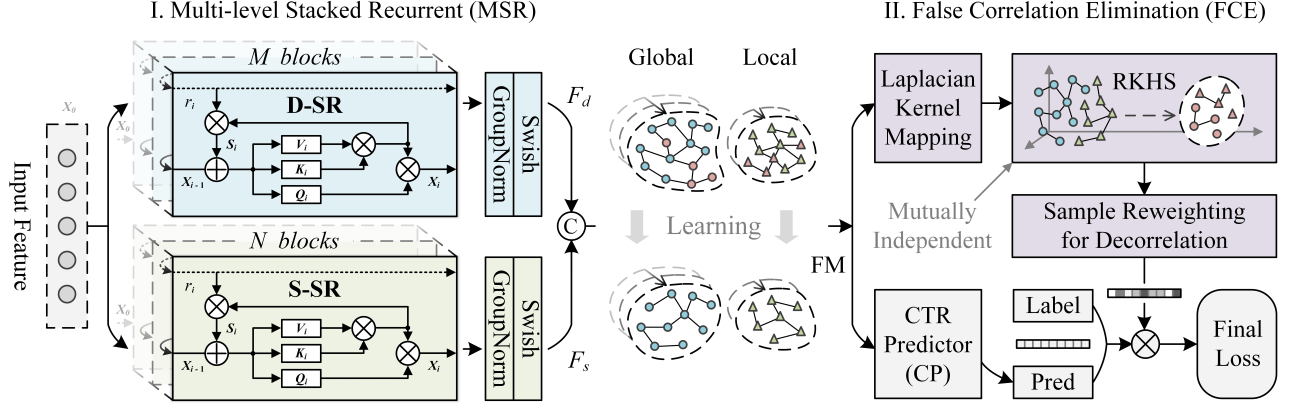


Figure 2: Overview of the REFORM framework, which contains two key components: I. the multi-level stacked recurrent (MSR) structure and II. the false correlation elimination (FCE) module. The deep and shallow stacked recurrent interactions (D-SR and S-SR) in the MSR structure and the FCE module are coloured blue, green, and purple, respectively. The D-SR and S-SR contain M and N ($M > N$) stacked blocks, and “ Q_i ”, “ K_i ”, and “ V_i ” denote query, key, and value for each block, respectively. The attenuation coefficient is denoted by r_i for each block (dotted lines). The outputs F_d and F_s are concatenated (“C”) as the input to the FCE and CTR predictor, which is visualized to show the false correlation elimination learning process guided by the FCE module. “RKHS” denotes the reproducing kernel Hilbert space. The FCE procedure is explained in the Algorithm 2.

3.2 False correlation elimination (FCE) First, we concatenate the last two outputs F_d , F_s to form a local feature map: $FM = \text{Concatenate}(F_d, F_s)$.

Statistical assessment of independence. To eliminate false correlations, we use sample reweighting to make false correlations independent of predicting users’ click behaviour: y_i . The theory behind it is elaborated in Section 3.5 and the supplemental materials. Specifically, inspired by the kernel function in the support vector machine (SVM), we first map the features into the high-dimensional space with the Laplacian kernel. In high-dimensional space, we eliminate the false correlation between features with nonlinear operations corresponding to the original feature space. We use X and Y to denote features, and the FCE measures the dependence between them. The theory of why FCE measures dependence is also given in the supplemental materials.

$$(3.3) \quad \text{FCE}(X, Y) = \|K_X - K_Y\|_{\text{FN}},$$

where $K_X = k_X(X, X)$ and $K_Y = k_Y(Y, Y)$ are Laplacian kernel matrices, $\|\cdot\|_{\text{FN}}$ is the Frobenius norm (FN) which corresponds to the Hilbert-Schmidt norm in Euclidean space [22], and k_X and k_Y are Laplacian kernels that can capture local patterns and are robust to outliers. However, applying the FCE approach with large-scale kernel matrices can be computationally expensive. Therefore, we use random Fourier features (RFF) to approximate the Laplacian kernel. Afterwards, the reconstructed features can be obtained in the new representation space, which reduces the time complexity from

Algorithm 2 Procedure of FCE module

Input: Balancing epoch number, Batch size

Output: Trained model with weight w_{result}

- 1: Define: n : the number of random Fourier space
 - 2: Initialize: sample weights: $w_{\text{result}} = [1, 1, \dots, 1]$
 - 3: Reload global features and weights as Eq.3.12, Eq.3.13
 - 4: **for** batch $\leftarrow 1$ **to** Batch size **do**
 - 5: **for** epoch balancing \leftarrow Balancing epoch number **to** 1 **do**
 - 6: $n_X = n_Y = \text{epoch balancing}$
 - 7: Optimize w_{result} with n_X and n_Y as Eq.3.11
 - 8: **end for**
 - 9: Back propagate with weighted prediction loss as Eq.3.18
 - 10: Save features and weights in GFI' and GWI' as Eq.3.14, Eq.3.15
 - 11: **end for**
-

$O(n^2)$ to $O(n)$.

$$(3.4) \quad \mathcal{H}_{\text{RFF}} = \{h : x \rightarrow \sqrt{2} \cos(wx + \phi) \mid w \sim N(0, 1), \phi \sim U(0, 2\pi)\},$$

where \mathcal{H}_{RFF} denotes the function space of RFF, w is sampled from the standard normal distribution and ϕ is sampled from the uniform distribution.

We define the partial cross-covariance matrix as the

measure of covariance between two sets of features:

$$(3.5) \quad \text{FCE}_{\text{RFF}}(X, Y) = \|C_{p(X), q(Y)}\|_{\text{FN}}^2$$

$$(3.6) \quad = \sum_{i=1}^{n_X} \sum_{j=1}^{n_Y} |\text{Cov}(p_i(X), q_j(Y))|^2,$$

where X and Y represent features, p and q are random Fourier feature mapping functions, n_X and n_Y are the number of functions from \mathcal{H}_{RFF} , $\|\cdot\|_{\text{FN}}$ is the Frobenius norm (FN), and $C_{p(X), q(Y)} \in \mathbb{R}^{n_X \times n_Y}$ is the cross-covariance matrix of random Fourier features $p(X)$ and $q(Y)$ containing entries:

$$(3.7) \quad p(X) = (p_1(X), \dots, p_n(X)), p_i(X) \in \mathcal{H}_{\text{RFF}}, \forall i,$$

$$(3.8) \quad q(Y) = (q_1(Y), \dots, q_n(Y)), q_j(Y) \in \mathcal{H}_{\text{RFF}}, \forall j.$$

Global sample weight optimization with consolidated features. In this section, we present a method for optimizing global features and global sample weights to enhance model performance. Our approach aims to effectively capture features and assign appropriate weights to samples. By iteratively updating feature weights and incorporating global and local information, we can improve the feature representation and their integration into the model. By minimizing $\text{FCE}_{\text{RFF}}^w(X, Y)$, we encourage feature independence, resulting in a more causal consistent covariate matrix. For any two features $X_{:,a}, X_{:,b} \in X$, the weighted false correlation elimination, are denoted as $\text{FCE}_{\text{RFF}}^w(X, Y)$.

$$(3.9) \quad \text{FCE}_{\text{RFF}}^w(X_{:,a}, X_{:,b}, w) = \sum_{i=1}^{n_X} \sum_{j=1}^{n_Y} |\text{Cov}(p_i(w^T X_{:,a}), q_j(w^T X_{:,b}))|^2.$$

In each iteration, our objective is to minimize the sum of Eq.3.9. Therefore, the result of weight is:

$$(3.10)$$

$$(3.11) \quad \begin{aligned} w_{\text{result}} &= \arg \min_w \sum_{1 \leq a \leq b \leq m} \text{FCE}_{\text{RFF}}^w(X_{:,a}, X_{:,b}, w) \\ &= \arg \min_w \sum_{1 \leq a \leq b \leq m} \sum_{i=1}^{n_X} \sum_{j=1}^{n_Y} |\text{Cov}(u_i, v_j)|^2, \end{aligned}$$

where $u_i = p_i(w^T X_{:,a})$, $v_j = q_j(w^T X_{:,b})$. To avoid local optima, we incorporate global information. We employ a remembrance module consisting of GFI and GWI. GFI captures global feature information, while

GWI stores global weight information. The features and weights are used to optimize the new sample weights.

$$(3.12) \quad \text{GFI}_i = \text{Concat}(\text{GFI}_{i-1}, \text{FM}_i),$$

$$(3.13) \quad \text{GWI}_i = \text{Concat}(\text{GWI}_{i-1}, w_i),$$

where $\text{GFI}_1 = \text{FM}_1$, $\text{GWI}_1 = w_1$, FM_i means the local feature information, w_i means local weight information, i means the number of iterations. We update the features and weights globally as follows:

$$(3.14) \quad \text{GFI}'_i = \frac{1}{2}(\text{GFI}'_{i-1} + \text{FM}_i),$$

$$(3.15) \quad \text{GWI}'_i = \frac{1}{2}(\text{GWI}'_{i-1} + w_i),$$

where $\text{GFI}'_1 = \frac{1}{2}\text{FM}_1$ and $\text{GWI}'_1 = \frac{1}{2}w_1$.

3.3 CTR predictor We divide the outputs F_d and F_s into k chunks, respectively, denoted as $F_d = [F_{d_1}, \dots, F_{d_k}]$, $F_s = [F_{s_1}, \dots, F_{s_k}]$, where k is a hyperparameter. F_{d_j} and F_{s_j} denote the j -th chunk feature of the D-SR output and S-SR output, respectively. We apply the CTR predictor (CP) to each paired chunk group consisting of F_{d_j} and F_{s_j} . The chunk computations are then aggregated using sum pooling to derive the final predicted probability:

$$(3.16) \quad \text{CP}(F_{d_j}, F_{s_j}) = b + w_{d_j}^T F_{d_j} + w_{s_j}^T F_{s_j} + F_{d_j}^T W_j F_{s_j},$$

$$(3.17) \quad \hat{y} = \sigma\left(\sum_{j=1}^k \text{CP}(F_{d_j}, F_{s_j})\right),$$

where w_{d_j} , w_{s_j} , and W_j are learnable weights, and σ is the sigmoid activation. Modelling the second-order interaction between hierarchical features $F_{d_j}^T W_j F_{s_j}$ is actually modelling arbitrary-order feature interaction.

3.4 Loss function We introduced a reweighting scheme for each sample within the commonly utilized binary cross-entropy loss. This involves applying a distinct weight to the loss of each sample during training.

$$(3.18) \quad L = - \sum_{i=1}^N w_{\text{result}_i} * (y_i \log(\hat{y}_i) + (1 - y_i) \log(1 - \hat{y}_i)),$$

where N is the number of examples, y_i is the true label, and \hat{y}_i is the predicted probability of a click. During training, we use the weight $w_{\text{result}} = [w_{\text{result}_1}, w_{\text{result}_2}, \dots, w_{\text{result}_N}]$ of the N Logloss values for every input sample calculated with the sample reweighting mechanism to conduct gradient descent.

Datasets	# Samples	# Fields	# Features
Criteo	45,840,617	39	2,086,936
Avazu	40,428,967	23	1,544,250
Frappe	288,609	10	5,382
MovieLens	2,006,859	3	90,445
UGC	1,015,236,921	92	10,640,310

Table 1: Statistics of the evaluation datasets.

3.5 The theory behind sample reweighting In the following part, we denote covariate features by $\text{FM}=[\text{FM}_{\text{rob}}, \text{FM}_{\text{fal}}]$, where FM_{rob} denotes the robust features and $\text{FM}_{\text{fal}} = \text{FM}/\text{FM}_{\text{rob}}$ denotes false correlation features. $g(\cdot)$ is a nonlinear function learned by the model with FM_{rob} and FM_{fal} . $\beta_{\text{FM}_{\text{rob}}}$ and $\beta_{\text{FM}_{\text{fal}}}$ denote the linear weights of FM_{rob} and FM_{fal} . [8] demonstrates that $\beta_{\text{FM}_{\text{fal}}}$ asymptotically exceeds 0, implying that models without the FCE module are inevitably suffer from the impact of false correlation features. Additionally, the correlation between FM_{rob} and $g(\text{FM}_{\text{rob}})$ exhibits less variation than the correlation between FM_{fal} and $g(\text{FM}_{\text{rob}})$ when exposed to parameter variance. Even when sample reweighting is applied randomly, the estimation of $\beta_{\text{FM}_{\text{rob}}}$ is more robust and less variable than the estimation of $\beta_{\text{FM}_{\text{fal}}}$.

When predicting y_i , we need y_i and FM_{fal} to be statistically independent of the minimal and optimal predictor FM_{rob} : $y_i \perp \text{FM}_{\text{fal}} | \text{FM}_{\text{rob}}$. To make FM_{rob} the minimal and optimal predictor, it has been proven that FM_{rob} is the minimal and optimal predictor if and only if FM_{rob} is the minimal robust feature set [29]. Therefore, we intend to capture the minimal robust feature set FM_{rob} to obtain robust prediction results. We denote the robust feature set as the minimal robust feature set for simplicity. Let \mathcal{W} be the set of sample weighting functions. Our objective is to acquire \mathcal{W}_{\perp} , a subset of \mathcal{W} , in which the features in FM are mutually independent. [33] proves that there exists a weight function $w \in \mathcal{W}$ that makes false correlations independent of y_i for linear models. Moreover, [28] proves whether data generation is linear or nonlinear, conducting a weighted least squares (WLS) operation using the weighting function in \mathcal{W}_{\perp} can lead to essentially perfect feature selection. Therefore, we transform the task from finding minimal robust features to obtaining independent FM by reweighting the samples.

4 Experiments

4.1 Datasets We conduct extensive experiments based on four official datasets and our production dataset. Table 1 provides an overview of the statistical information for the different datasets.

Criteo¹. Criteo is a dataset for online advertising and CTR prediction, including real-world display ads.

Avazu². Avazu is a widely used dataset in CTR prediction and online advertising research. This dataset includes real-world advertising data, focusing on mobile ads and user demographics.

Frappe³. Frappe is a popular dataset in human activity recognition research, including sensor data captured with smartphones.

MovieLens⁴. MovieLens is used in recommender systems and contains movie ratings and user information.

User Game Content (UGC). The UGC dataset consists of the user game content clicking behavior data collected from our online service within a month. We collect clicking logs with the anonymous user ID, user behaviour history, game content features (e.g., categories), and context features (e.g., operation time).

4.1.1 Evaluation metrics We utilize two evaluation metrics, the area under the ROC curve (AUC) and the Logloss (cross-entropy), in the experiments.

4.1.2 Baseline To fairly and accurately verify the improvement achieved by the proposed MSR structure and FCE module, we use a two-stream MLP network as the “Baseline” method. The MLP sizes of the two branches are set to [400, 400, 400] and [800], respectively, which achieves the best performance. This approach aligns with established best practices for two-stream CTR models [13], providing a solid foundation for evaluating any modifications or novel approaches in a controlled manner.

4.1.3 Implementation For fair comparisons with recent state-of-the-art (SOTA) methods, we use the preprocessed datasets released by [2] with the same split and preprocessing procedure. All models and experiments are implemented based on the FuxiCTR toolkit [35]. REFORM and the “Baseline” model follow the same experimental settings as FinalMLP [13], with the batch size for all datasets set to 4,096, the embedding size set to 10 for the five datasets, and the learning rate set to 0.001 unless specified. The number of chunks k in CP is set to 50 for Criteo and UGC, 10 for Avazu and MoiveLens, and 1 for Frappe, respectively. The remaining hyperparameters were kept constant for the five datasets. To mitigate overfitting, we implement early stopping based on the AUC obtained with the validation dataset. In the REFORM model, take D-

¹<http://labs.criteo.com>

²<https://www.kaggle.com>

³<https://github.com/openbenchmark/BARS>

⁴<https://github.com/openbenchmark/BARS>

Class	Model	Criteo		Avazu		MovieLens		Frappe	
		AUC \uparrow	Logloss \downarrow	AUC \uparrow	Logloss \downarrow	AUC \uparrow	Logloss \downarrow	AUC \uparrow	Logloss \downarrow
First-Order	LR [18]	0.7874	0.4551	0.7574	0.3944	0.9449	0.2870	0.9394	0.2407
Second-Order	FM [17]	0.8028	0.4514	0.7618	0.3910	0.9551	0.2328	0.9707	0.2003
	AFM [27]	0.8050	0.4434	0.7598	0.3921	0.9568	0.2224	0.9612	0.2182
High-Order	HOFM (3rd) [1]	0.8052	0.4456	0.7690	0.3873	0.9573	0.2075	0.9701	0.2006
	NFM [7]	0.8072	0.4444	0.7708	0.3876	0.9682	0.2064	0.9765	0.1694
	OPNN [15]	0.8096	0.4426	0.7718	0.3838	0.9566	0.2333	0.9812	0.1912
	CIN [12]	0.8086	0.4437	0.7739	0.3839	0.9666	0.2066	0.9796	0.1676
	AutoInt [21]	0.8125	0.4396	0.7748	0.3834	0.9656	0.2440	0.9791	0.1853
	AFN [2]	0.8135	0.4386	0.7730	0.3863	0.9616	0.2523	0.9801	0.1852
	SAM [3]	0.8128	0.4392	0.7725	0.3868	0.9633	0.2155	0.9743	0.2315
Ensemble	DCN [24]	0.8106	0.4414	0.7749	0.3855	0.9630	0.2162	0.9753	0.1676
	DeepFM [6]	0.8130	0.4389	0.7752	0.3859	0.9625	0.2520	0.9759	0.1993
	xDeepFM [12]	0.8127	0.4392	0.7747	0.3841	0.9612	0.2186	0.9779	0.1869
	DRIN [10]	0.8136	0.4383	0.7729	0.3860	0.9703	0.1998	0.9812	0.1592
	MaskNet [26]	0.8137	0.4381	0.7731	0.3859	0.9706	0.1992	0.9819	0.1586
	DCN-V2 [25]	0.8139	0.4382	0.7737	0.3840	0.9675	0.2131	0.9778	0.1910
	FINAL [34]	0.8133	0.4393	0.7754	0.3837	0.9708	0.1996	0.9830	0.1567
	FinalMLP [13]	0.8140	0.4380	0.7756	0.3831	0.9713	0.1989	0.9836	0.1546
Ours	REFORM	0.8149**	0.4370**	0.7775**	0.3812**	0.9724**	0.1956**	0.9857**	0.1501**

Table 2: Overall performance of the SOTA CTR models. The t-test results show that our performance advantage over previous SOTA methods is statistically significant based on four datasets ($\star: p < 10^{-2}$, $\star\star: p < 10^{-4}$).

Model	Criteo		Avazu		UGC	
	AUC \uparrow	Logloss \downarrow	AUC \uparrow	Logloss \downarrow	AUC \uparrow	Logloss \downarrow
Previous SOTA (FinalMLP)	0.8140	0.4380	0.7756	0.3831	0.8039	0.4052
Baseline	0.8138	0.4387	0.7752	0.3845	0.8035	0.4059
Baseline + MSR	0.8144	0.4376	0.7764	0.3827	0.8046	0.4044
Baseline + FCE	0.8147	0.4373	0.7770	0.3818	0.8053	0.4035
Full Approach (REFORM)	0.8149**	0.4370**	0.7775**	0.3812**	0.8058**	0.4027**

Table 3: Ablation study of the proposed REFORM model based on the Criteo, Avazu, and UGC datasets.

SR as an example, we define the attenuation coefficient r as $[\frac{31}{32}, \frac{63}{64}, \dots, \frac{2^{M+5}-1}{2^{M+5}}]$.

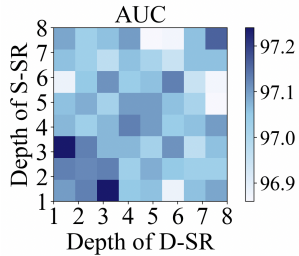


Figure 3: Performance with different MSR depths.

4.2 Comparison with SOTA methods The performance of our REFORM framework is compared with that of eighteen competitive approaches. Detailed de-

scriptions of the methods are included in the supplemental materials. We classify these methods into four categories: first-order, second-order, high-order, and ensemble. We ran REFORM with every dataset 5 times and reported the average results. Then we conducted t-tests to compare the performance of REFORM with that of the other methods, and the results are summarized in Table 2. For all four datasets, REFORM outperforms all other models in terms of both AUC and Logloss, which validates its generalization ability. The greatest improvement is observed with the Avazu dataset, where REFORM shows a relative improvement of 0.19% over the second-best performing model. Previous two-stream nonlinear interaction-based methods such as [13] show robust performance across all datasets among the ensemble methods, while our REFORM constructs more effective multi-level features with false correlation elimination and achieves the 1st-ranked performance.

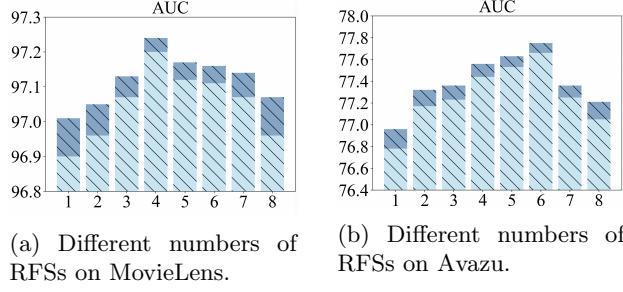


Figure 4: Comparison of using fixed number (light blue) and decreasing numbers (dark blue) of RFS.

4.3 Ablation study We verify the effectiveness of the MSR and FCE through extensive experiments.

Accuracy improvement with the MSR and FCE. Table 3 shows that the MSR and FCE stably improve model performance, and the improvement is notably significant on the production dataset (UGC), exceeding the “Baseline” method by 0.23% AUC. “Baseline + MSR” denotes that the two-stream MLP network is replaced by the MSR, and the superior performance on all three datasets demonstrates that the multi-level features constructed by our MSR are more comprehensive.

Speed improvement with the MSR. The rapid inference speed of REFORM is attributed to the MSR structure while the FCE does not affect the inference speed because the FCE is only used during training. We choose the “Baseline” model and the cutting-edge ensemble class models, FinalMLP [13] and DRIN [10], as comparisons. Table 4 demonstrates that REFORM significantly outperforms previous SOTA methods in inference speed (almost $3\times$ faster than FinalMLP).

Model	Avazu	MovieLens	UGC
Baseline	35	1.4	96
FinalMLP	30	1.1	87
DRIN	16	0.8	50
REFINE	10	0.4	24

Table 4: Inference time(s) comparison on the test set.

Different depths of D-SR and S-SR. We verified the performance of REFORM with different combinations of S-SR and D-SR at various depths. For the five datasets, the best performance of REFORM is obtained with D-SR and S-SR depths of 3 and 1, respectively. Figure 3 shows a visualization example based on the MovieLens dataset. When the D-SR and S-SR depths are the same (1, 2, and 3), the performance is similar to that of the “Baseline” method (97.10, 97.12, and 97.07 vs. 97.11), which shows that the MSR is not able to

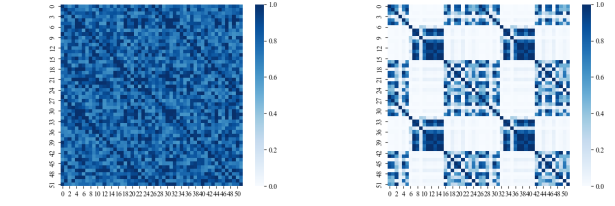


Figure 5: False correlation elimination of REFORM.

construct multi-level features with the same stacking depth to improve performance. When the depths of D-SR and S-SR are set to 3 and 1, the result is 0.10% higher than that of the “Baseline” method.

Different numbers of random Fourier space (RFS). We analyze the influence of using different numbers of RFSs. In Figure 4, the light blue columns show the different AUCs of using different fixed numbers of RFSs (1~8) on MovieLens and Avazu. Through extensive experiments, we further find that compared to a fixed number of RFSs, using decreasing numbers of RFSs in each epoch further improves performance. The dark blue columns show performance with decreasing numbers of RFSs, and the horizontal axis represents the maximum value (the number of RFSs is uniformly decreasing from the maximum value to 1 in each epoch).

Feature visualization for FCE. We randomly select variables with 50 dimensions from input features of the CTR predictor learned by “Baseline” and FCE. Figure 5 shows that after applying FCE, the correlations among features have been significantly eliminated, while model performance is notably improved. To a certain extent, this underscores the capacity of FCE to extract valuable correlations pertinent to the CTR task while eliminating a plethora of extraneous and false correlations. More experiments are reported in the supplemental materials.

5 Conclusion

We propose the REFORM for CTR prediction. A multi-level stacked recurrent (MSR) structure is proposed that enables the network to efficiently capture global and local high-order representations based on the constructed deep and shallow feature spaces. A false correlation elimination (FCE) module is introduced that effectively removes false correlations, allowing the model to focus on the true causal effects. Extensive experiments on four public datasets and our production dataset show the SOTA performance of REFORM, which advances CTR prediction methodologies and offers valuable insights for future research and applications.

References

- [1] M. Blondel, A. Fujino, N. Ueda, and M. Ishihata. Higher-order factorization machines. *NeurIPS*, 29, 2016.
- [2] W. Cheng, Y. Shen, and L. Huang. Adaptive factorization network: Learning adaptive-order feature interactions. In *AAAI*, volume 34, pages 3609–3616, 2020.
- [3] Y. Cheng and Y. Xue. Looking at ctr prediction again: Is attention all you need? In *SIGIR*, pages 1279–1287, 2021.
- [4] S. Dou, R. Zheng, T. Wu, S. Gao, J. Shan, Q. Zhang, Y. Wu, and X. Huang. Decorrelate irrelevant, purify relevant: Overcome textual spurious correlations from a feature perspective. *arXiv preprint*, 2022.
- [5] H. Du, Y. Li, Y. Sun, J. Zhu, and F. Tombari. Srhnet: Stacked recurrent hourglass network for stereo matching. *IEEE Robotics and Automation Letters*, 6(4):8005–8012, 2021.
- [6] H. Guo, R. Tang, Y. Ye, Z. Li, and X. He. Deepfm: a factorization-machine based neural network for ctr prediction. *arXiv preprint*, 2017.
- [7] X. He and T.-S. Chua. Neural factorization machines for sparse predictive analytics. In *SIGIR*, pages 355–364, 2017.
- [8] Y. He, X. Shen, R. Xu, T. Zhang, Y. Jiang, W. Zou, and P. Cui. Covariate-shift generalization via random sample weighting. *AAAI*, 2023.
- [9] Y. Juan, Y. Zhuang, W.-S. Chin, and C.-J. Lin. Field-aware factorization machines for ctr prediction. In *RecSys*, pages 43–50, 2016.
- [10] X. Jun, Z. Xudong, X. Xinying, H. Xiaoxia, R. Jinchang, and L. Xingbing. Drin: Deep recurrent interaction network for click-through rate prediction. *Information Sciences*, 604:210–225, 2022.
- [11] Y. Li, H. Chen, J. Tan, and Y. Zhang. Causal factorization machine for robust recommendation. In *JCDL*, pages 1–9, 2022.
- [12] J. Lian, X. Zhou, F. Zhang, Z. Chen, X. Xie, and G. Sun. xdeepfm: Combining explicit and implicit feature interactions for recommender systems. In *SIGKDD*, pages 1754–1763, 2018.
- [13] K. Mao, J. Zhu, L. Su, G. Cai, Y. Li, and Z. Dong. Finalmlp: An enhanced two-stream mlp model for ctr prediction. *arXiv preprint*, 2023.
- [14] J. Pan, J. Xu, A. L. Ruiz, W. Zhao, S. Pan, Y. Sun, and Q. Lu. Field-weighted factorization machines for click-through rate prediction in display advertising. In *WWW*, pages 1349–1357, 2018.
- [15] Y. Qu, H. Cai, K. Ren, W. Zhang, Y. Yu, Y. Wen, and J. Wang. Product-based neural networks for user response prediction. In *ICDM*, pages 1149–1154, 2016.
- [16] P. Ramachandran, B. Zoph, and Q. V. Le. Swish: a self-gated activation function. *arXiv preprint*, 2017.
- [17] S. Rendle. Factorization machines. In *ICDM*, pages 995–1000. IEEE, 2010.
- [18] M. Richardson, E. Dominowska, and R. Ragno. Predicting clicks: estimating the click-through rate for new ads. In *WWW*, pages 521–530, 2007.
- [19] Z. Shen, P. Cui, T. Zhang, and K. Kunag. Stable learning via sample reweighting. In *AAAI*, 2020.
- [20] M. Shoenberger, M. Patwary, R. Puri, P. LeGresley, J. Casper, and B. Catanzaro. Megatron-lm: Training multi-billion parameter language models using model parallelism. *arXiv preprint*, 2019.
- [21] W. Song, C. Shi, Z. Xiao, Z. Duan, Y. Xu, M. Zhang, and J. Tang. AutoInt: Automatic feature interaction learning via self-attentive neural networks. In *CIKM*, pages 1161–1170, 2019.
- [22] E. V. Strobl, K. Zhang, and S. Visweswaran. Approximate kernel-based conditional independence tests for fast non-parametric causal discovery. *Journal of Causal Inference*, 7(1):20180017, 2019.
- [23] Y. Sun, J. Pan, A. Zhang, and A. Flores. Fm2: Field-matrixed factorization machines for recommender systems. In *WWW*, pages 2828–2837, 2021.
- [24] R. Wang, B. Fu, G. Fu, and M. Wang. Deep & cross network for ad click predictions. In *ADKDD*, pages 1–7, 2017.
- [25] R. Wang, R. Shivanna, D. Cheng, S. Jain, D. Lin, L. Hong, and E. Chi. Dcn v2: Improved deep & cross network and practical lessons for web-scale learning to rank systems. In *WWW*, pages 1785–1797, 2021.
- [26] Z. Wang, Q. She, and J. Zhang. Masknet: Introducing feature-wise multiplication to ctr ranking models by instance-guided mask. *arXiv preprint*, 2021.
- [27] J. Xiao, H. Ye, X. He, H. Zhang, F. Wu, and T.-S. Chua. Attentional factorization machines: Learning the weight of feature interactions via attention networks. *arXiv preprint*, 2017.
- [28] R. Xu, P. Cui, Z. Shen, X. Zhang, and T. Zhang. Why stable learning works? a theory of covariate shift generalization. *arXiv preprint*, 2021.
- [29] R. Xu, X. Zhang, Z. Shen, T. Zhang, and P. Cui. A theoretical analysis on independence-driven importance weighting for covariate-shift generalization. In *ICML*, pages 24803–24829. PMLR, 2022.
- [30] Y. Xu, Y. Zhu, F. Yu, Q. Liu, and S. Wu. Disentangled self-attentive neural networks for click-through rate prediction. In *CIKM*, pages 3553–3557, 2021.
- [31] L. Yao, Z. Chu, S. Li, Y. Li, J. Gao, and A. Zhang. A survey on causal inference. *TKDD*, 15(5):1–46, 2021.
- [32] X. Zhang, P. Cui, R. Xu, L. Zhou, Y. He, and Z. Shen. Deep stable learning for out-of-distribution generalization. In *CVPR*, pages 5372–5382, 2021.
- [33] X. Zhou, Y. Lin, R. Pi, W. Zhang, R. Xu, P. Cui, and T. Zhang. Model agnostic sample reweighting for out-of-distribution learning. In *ICML*, pages 27203–27221. PMLR, 2022.
- [34] J. Zhu, Q. Jia, G. Cai, Q. Dai, J. Li, Z. Dong, R. Tang, and R. Zhang. Final: Factorized interaction layer for ctr prediction. In *SIGIR*, pages 2006–2010, 2023.
- [35] J. Zhu, J. Liu, S. Yang, Q. Zhang, and X. He. Open benchmarking for click-through rate prediction. In *CIKM*, pages 2759–2769, 2021.